Electronic Supplementary Material (ESI) for Environmental Science: Nano.

Supporting Information

for

3D hierarchical defect-rich C@MoS_2 nanosheet arrays developed on montmorillonite with enhanced performance on Pb(II) removal

Lin Tan[1,‖], Yunsong Liu[1,2,‖], Fanling Meng[1], Pengfei Wu[1], Yunxue Xia[1], Yuanyuan Tang[1,*]

1. School of Environmental Science and Engineering, Guangdong Provincial Key Laboratory of Soil and Groundwater Pollution Control, State Environmental Protection Key Laboratory of Integrated Surface Water-Groundwater Pollution Control, Southern University of Science and Technology, 1088 Xueyuan Blvd, Nanshan District, Shenzhen 518055, P. R. China

2. College of Urban and Environmental Sciences, Peking University, Beijing 100871, P. R. China

[*]Corresponding author, E-mail address: tangyy@sustech.edu.cn

[‖]Both authors contributed equally to this article.

Including 3 Tables and 10 Figures in 14 pages

Table S1 Chemical weight (g) and experimental conditions for C@MoS_2/MMT fabrication, as well as MoS_2 and C content in the composites.

Chemical weight /g				**Experimental conditions**		**Composite content /%**	
Hexaammonium molybdate	Montmorillonite	Thiourea	Glucose	Temperature /°C	Time /h	MoS_2	C
0.415	0.400	0.380	-	200	24	22.97	1.11
0.415	0.400	0.380	0.200	200	24	27.62	4.36
0.415	0.400	0.380	0.600	200	24	23.89	12.54
0.415	0.400	0.380	1.000	200	24	21.75	19.73
0.415	0.400	0.380	0.600	180	24	18.85	14.47
0.415	0.400	0.380	0.600	220	24	28.61	11.40

Table S2 Modelling parameters of the kinetic and isotherm study on Pb(II) adsorption

Adsorption kinetics	pseudo-first-order		Q_e (mg/g)	61.95
			K_1 (min^{-1})	8.8×10^{-3}
			R^2	0.837
	pseudo-second-order		Q_e (mg/g)	200.0
			K_2 (mg/(g·min))	5.81×10^{-4}
			R^2	0.999
	Intraparticle diffusion	Stage 1	K_{p-1} (mg/(g·$min^{1/2}$))	13.679
			C_1 (mg/g)	69.47
			R^2	0.950
		Stage 2	K_{p-2} (mg/(g·$min^{1/2}$))	1.822
			C_2 (mg/g)	138.33
			R^2	0.970
Adsorption isotherms	Langmuir model		Q_m (mg/g)	187.0
			K_L (L/mg)	1.742
			R^2	0.995
	Freundlich model		n	10.088
			K_F (mg/g)·$(L/mg)^{1/n}$	118.5
			R^2	0.985

Q_e (mg/g) is the adsorption capacity at equilibrium. K_1, K_2 and K_p are the pseudo-first order kinetic rate constant (min^{-1}), pseudo-second order kinetic rate constant (mg/(g·min)) and intra-particle diffusion kinetic rate constant (mg/(g·$min^{1/2}$)), respectively. C is a constant related the resistance to the mass transfer in the surface. Q_m and K_L refer to the maximum adsorption capacity and the Langmuir constant (L/mg), respectively. K_F (mg/g)·$(L/mg)^{1/n}$ and $1/n$ are Freundlich constants, indicating the adsorption capacity and intensity, respectively.

Table S3 Comparison of Pb(II) adsorption capacity (mg/g) between the C@MoS_2/MMT in this study and other adsorbents.

Adsorbents	Q_m (mg/g)	References*
C@MoS_2/MMT	**187**.0	**This work**
Polyamide-amine dendritic magnetic halloysite	194.4	1
Graphene oxide-montmorillonite nanocomposite	19.8	2
FSBP ($Fe_3O_4/Sr_{5x}Ba_{3x}(PO_4)_3(OH)$)	143.7	3
Activated carbon supported nanoscale zero-valenst iron	59.4	4
Nanodiamond/MoS_2	19.9	5
Magnetic graphene oxide grafted polymaleicamide dendrimer	181.4	6
Fe_3O_4@DAPF	83.3	7
Lipopeptides modified Na-montmorillonite	20.3	8
Montmorillonite	57.0	9

*Reference list for this table:

1. D. K. Cheng, X. H. Dai, L. Chen, Y. H. Cui, C. W. Qiang, Q. Sun and J. D. Dai, Thiol-yne click synthesis of polyamide-amine dendritic magnetic halloysite nanotubes for the efficient removal of Pb(II), *ACS Sustainable Chem. Eng.*, 2020, **8**, 771-781.
2. C. Y. Zhang, J. D. Luan, X. K.Yu and W. Chen, Characterization and adsorption performance of graphene oxide-montmorillonite nanocomposite for the simultaneous removal of Pb^{2+} and p-nitrophenol, *J. Hazard. Mater.*, 2019, **378**, 120739.
3. F. Zhang, X. X. Tang, Y. X. Huang, A. A. Keller and J. Lan, Competitive removal of Pb^{2+} and malachite green from water by magnetic phosphate nanocomposites, *Water Res.*, 2019, **150**, 442-451.
4. X. J. Liu, D. G. Lai and Y. Wang, Performance of Pb(II) removal by an activated carbon supported nanoscale zero-valent iron composite at ultralow iron content, *J. Hazard. Mater.*, 2019, **361**, 37-48.
5. N. Baghban, E. Yilmaz and M. Soylak, Nanodiamond/MoS_2 nanorod composite as a novel sorbent for fast and effective vortex-assisted micro solid phase extraction of lead(II) and copper(II) for their flame atomic absorption spectrometric detection, *J. Mol. Liq.*, 2017, **234**, 260-267.
6. Y. X. Ma, Y. L. Kou, D. Xing, P. S. Jin, W. J. Shao, X. Li and P. Q. La, Synthesis of magnetic graphene oxide grafted polymaleicamide dendrimer nanohybrids for adsorption of Pb(II) in aqueous solution, *J. Hazard. Mater.*, 2017, **340**, 407-416.
7. S. Venkateswarlu and M. Yoon, Core-shell ferromagnetic nanorod based on amine polymer composite (Fe_3O_4@DAPF) for fast removal of Pb(II) from aqueous solutions, *ACS Appl. Mater. Interfaces*, 2015, **7**, 25362-25372.
8. Z. Zhu, C. Gao, Y. L. Wu, L. F. Sun, X. L. Huang, W. Ran and Q. R. Shen, Removal of heavy metals from aqueous solution by lipopeptides and lipopeptides modified Na-montmorillonite, *Bioresour. Technol.*, 2013, **147**, 378-386.
9. S. Q. Zhang and W. G. Hou, Adsorption behavior of Pb(II) on montmorillonite, *Colloids Surf., A.*, 2008, **320**, 92-97.

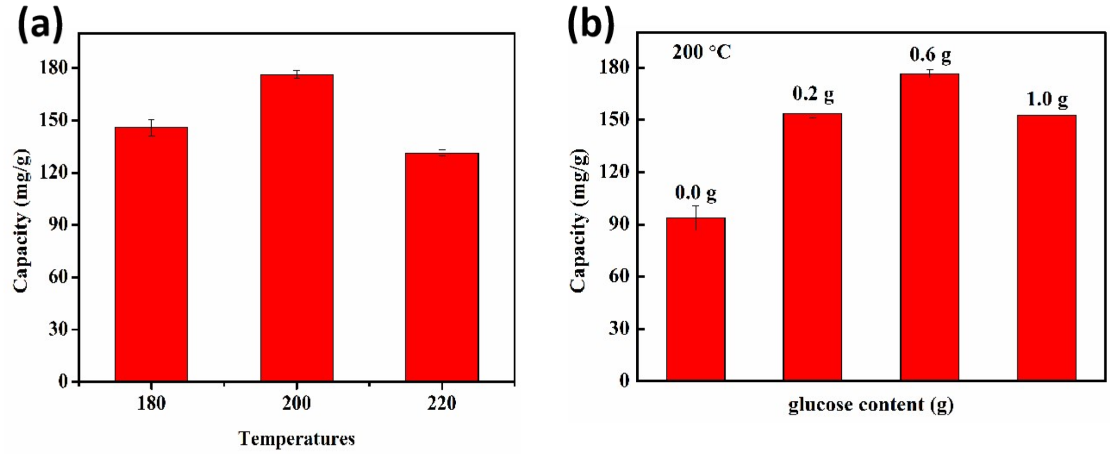

Fig. S1 The Pb(II) adsorption capacity of the C@MoS_2/MMT composites fabricated (a) at different temperatures and (b) with different glucose content.

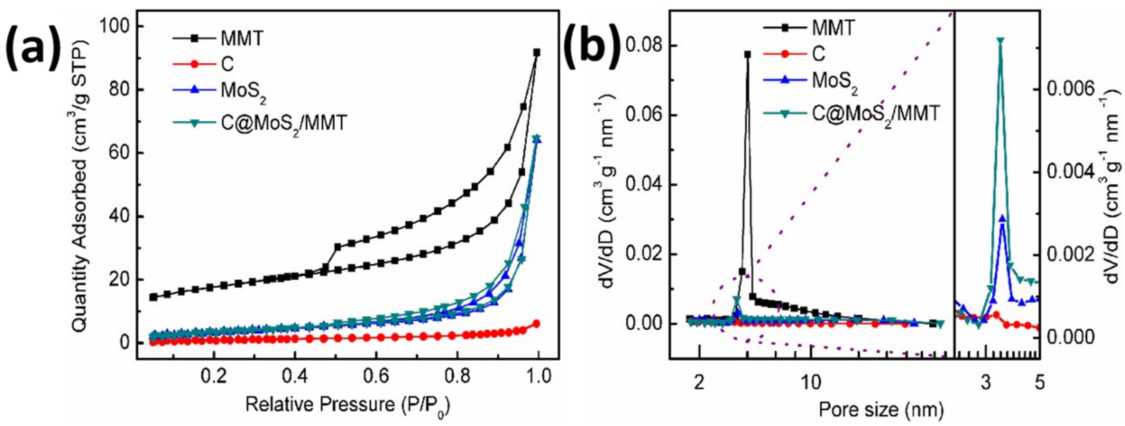

Fig. S2 (a) Nitrogen adsorption-desorption isotherm and (b) BJH pore-size distribution of MMT, C, MoS_2 and C@MoS_2/MMT.

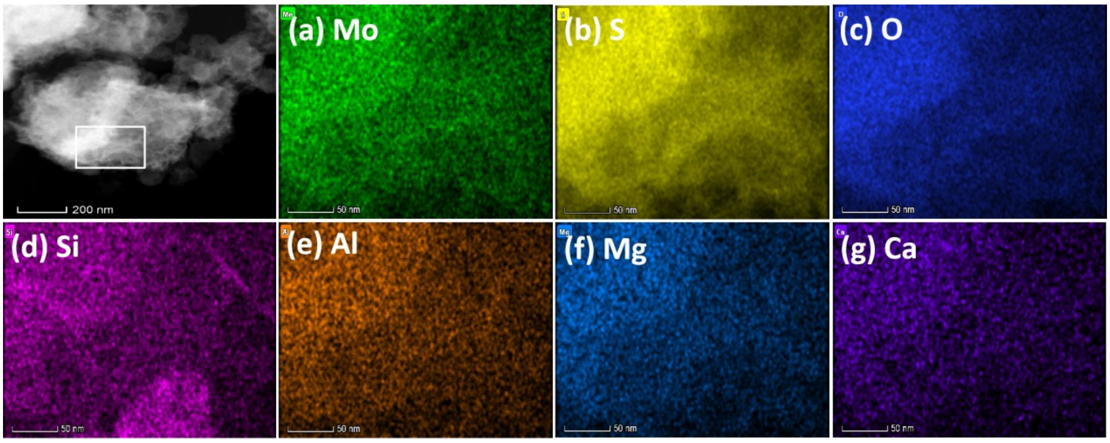

Fig. S3 Element mapping of the C@MoS_2/MMT hybrid composite by TEM.

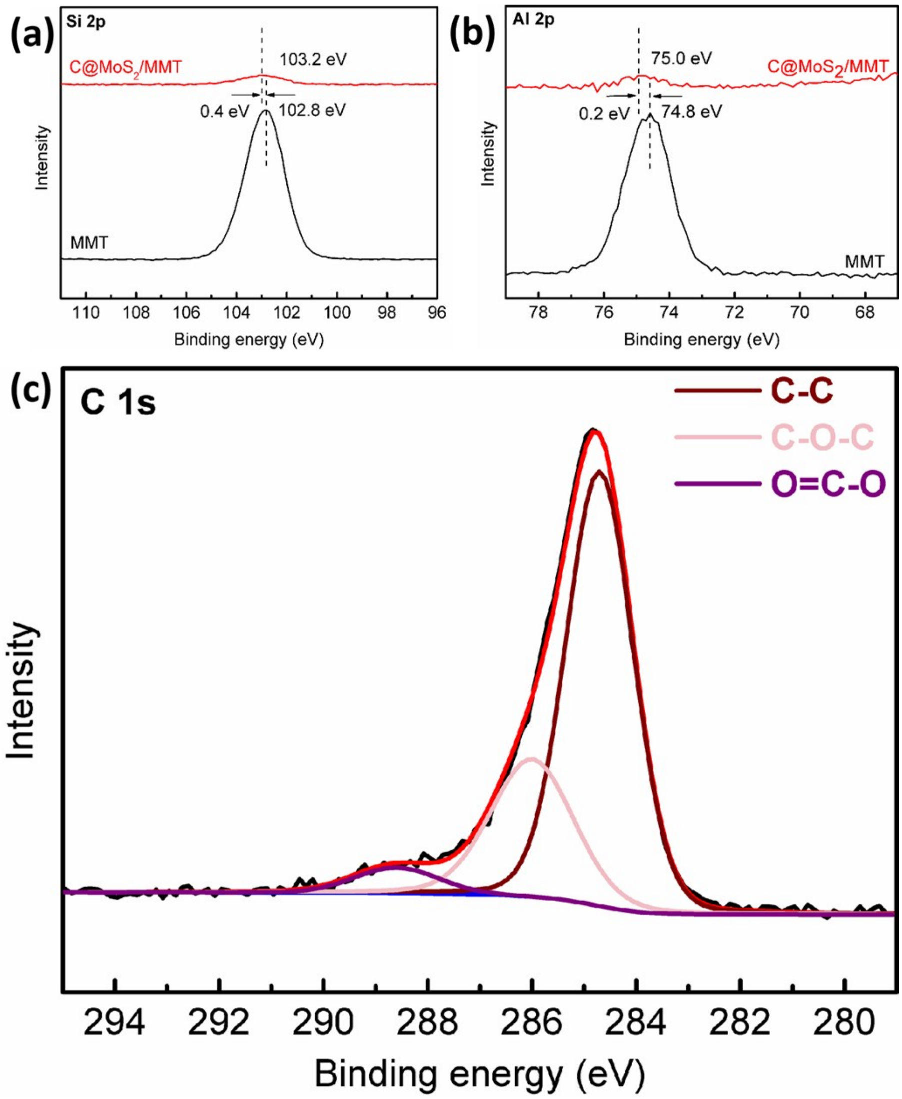

Fig. S4 High-resolution XPS spectra for (a) Si 2p and (b) Al 2p electrons of the raw MMT and C@MoS_2/MMT, (c) C 1s of C@MoS_2/MMT.

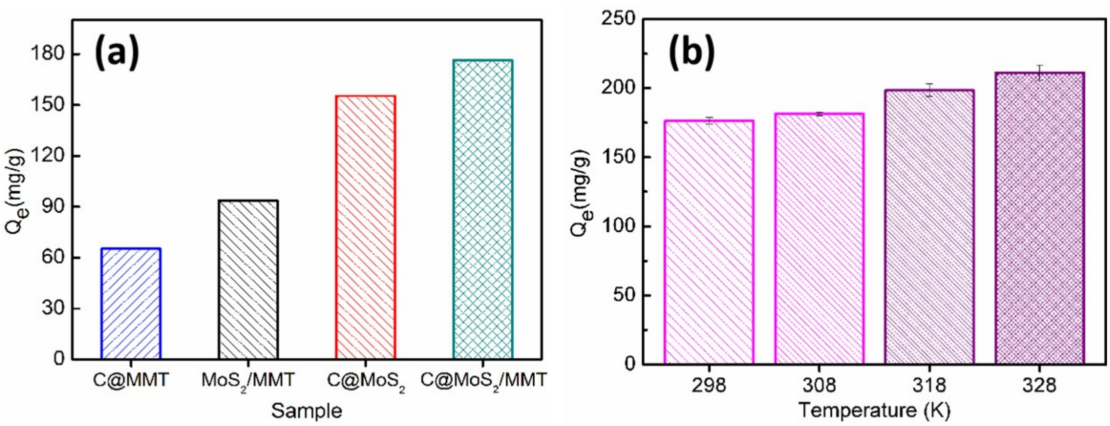

Fig. S5 (a) Pb(II) adsorption capacity of C@MMT, MoS_2/MMT, C@MoS_2, and C@MoS_2/MMT; (b) Effect of temperatures on Pb(II) adsorption by C@MMT/MoS_2.

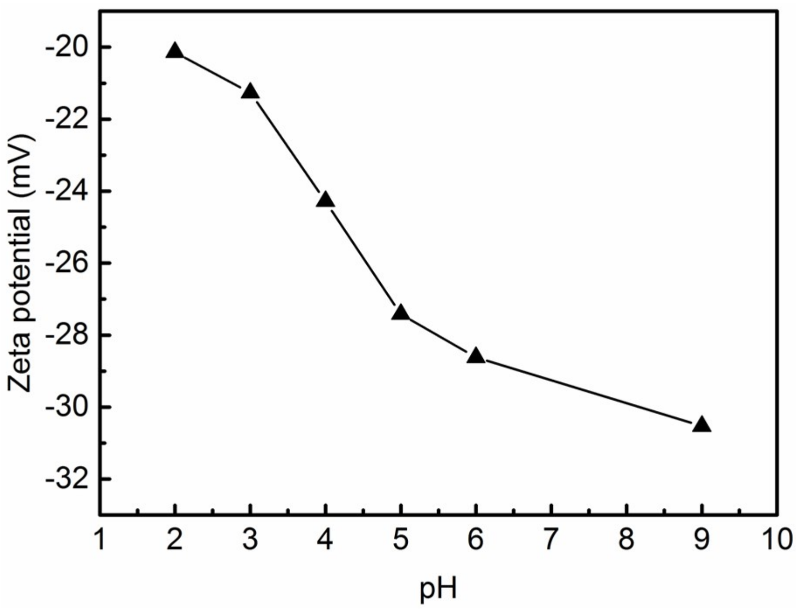

Fig. S6 Zeta potential of C@MMT/MoS_2.

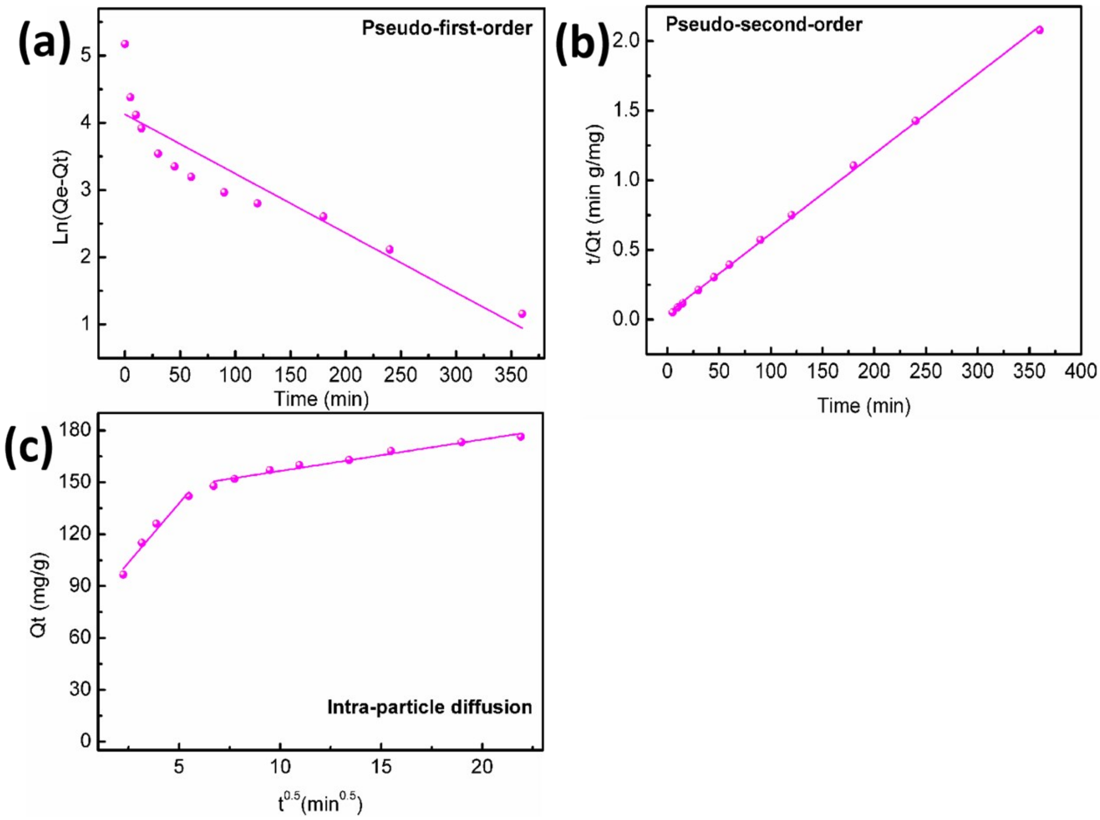

Fig. S7 The linear fitting plots of pseudo-first-order, pseudo-second-order and intra-particle diffusion models for the adsorption kinetic of Pb(II) by C@MMT/MoS_2.

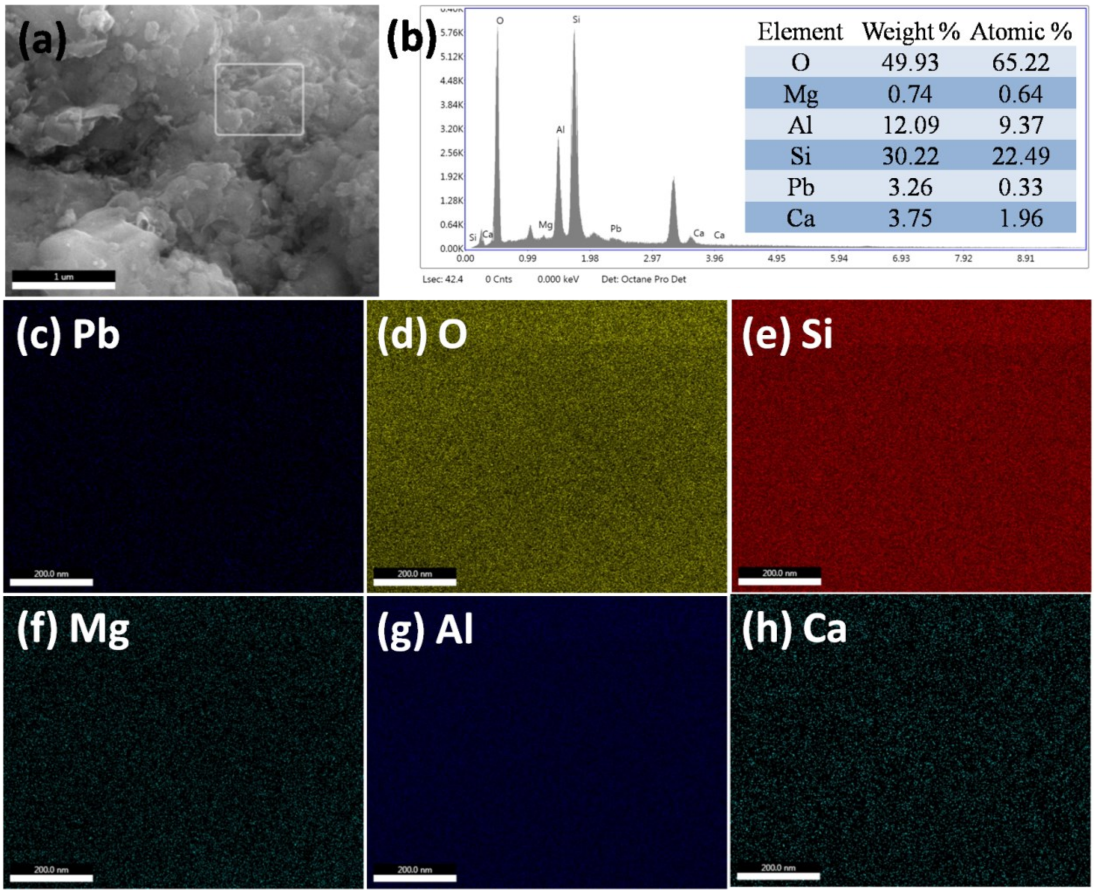

Fig. S8 (a) SEM image, (b) EDS spectrum and (c-h) elemental mapping images of MMT after Pb(II) adsorption.

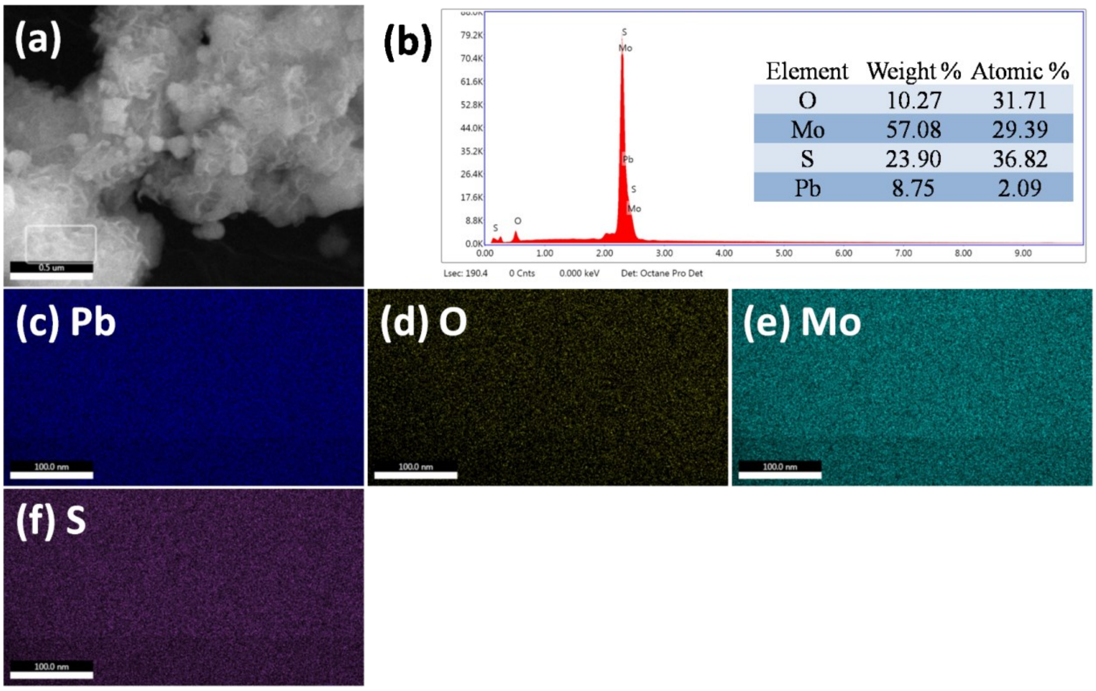

Fig. S9 (a) SEM image, (b) EDS spectrum and (c-f) elemental mapping images of MoS_2 after Pb(II) adsorption.

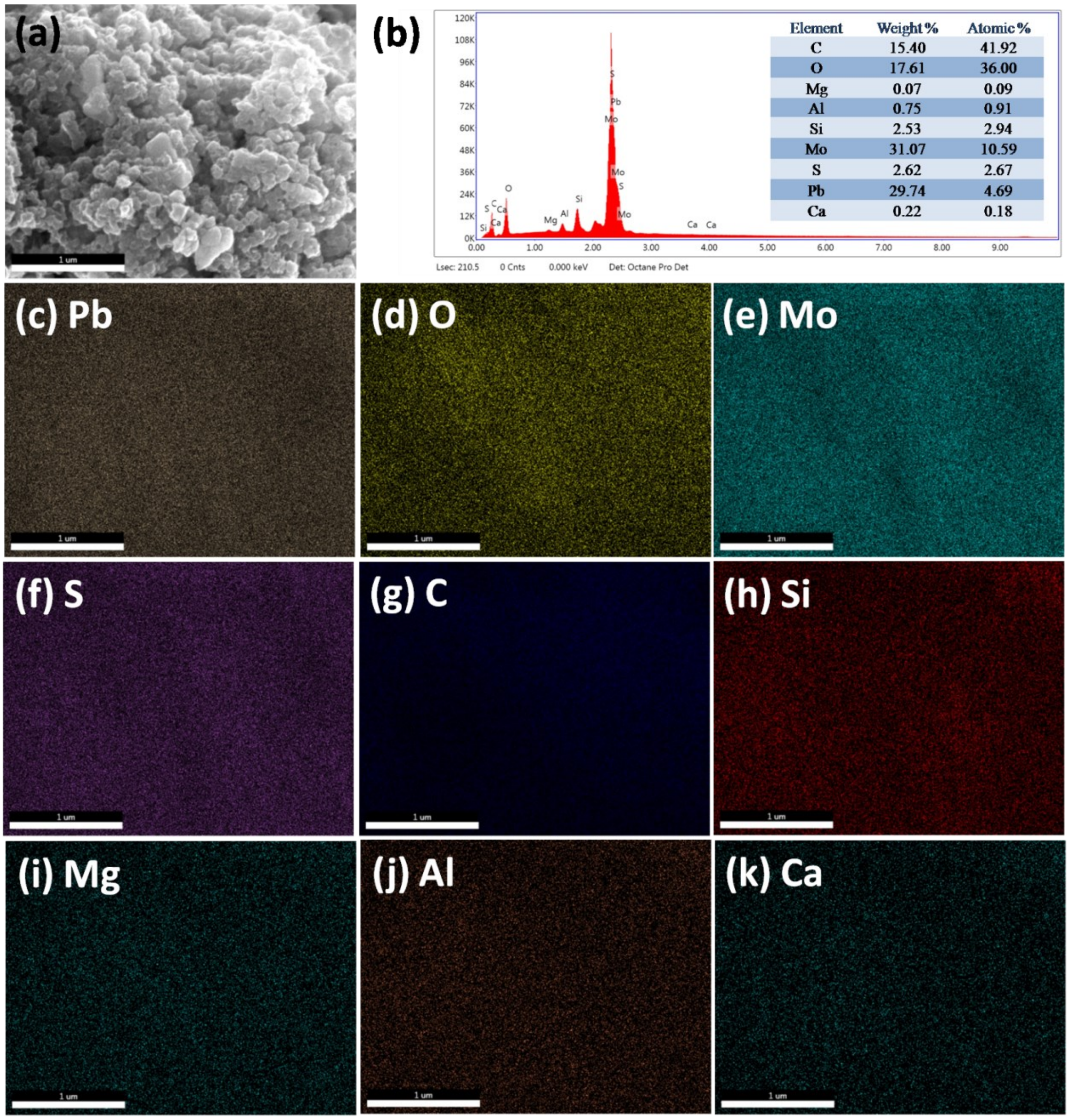

Fig. S10 (a) SEM image, (b) EDS spectrum and (c-k) elemental mapping images of C@MoS_2/MMT after Pb(II) adsorption.